J. Fluid Mech. (1992), *vol.* 241, *pp.* 615–643
Printed in Great Britain

The nonlinear evolution of a slowly growing wave on a laterally sheared baroclinic flow

By M. J. BELL

Short-Range Forecasting Division, Room H021, Hadley Centre, UK Meteorological Office, London Road, Bracknell, RG12 2SZ, UK

(Received 22 April 1991 and in revised form 4 February 1992)

Wave disturbances to baroclinic flows produce cyclones in the atmosphere and eddies in the oceans and have been extensively studied in laboratory experiments with differentially heated annuli of rotating fluid. Related analytical studies have concentrated mainly on the development of slowly growing waves on laterally uniform zonal flows. Neutral inviscid waves on such flows do not advect their own potential vorticity field whereas neutral waves on most laterally sheared baroclinic flows do. Scaling arguments suggest that on these laterally sheared flows the harmonics generated by the neutral waves play the dominant role in arresting the initial growth of weakly unstable waves. The arrest of a wave is chiefly accomplished by fully nonlinear advection within a critical layer centred on the wave's steering level whose depth is proportional to the wave's amplitude. Explicit numerical solutions illustrating these points are presented for a case in which the critical level is non-singular and the inviscid calculations comparatively straightforward. The stability of the solutions and the effects of diffusive fluxes on them are discussed. Potential vorticity diagnostics for a numerical simulation of a wave flow in a rotating annulus near the axisymmetric transition show that distortion of the wave's potential vorticity field is mainly confined to the vicinity of the steering level. Assumptions and approximations made in the explicit calculations which are of doubtful validity for this flow are highlighted.

1. Introduction

The growth and equilibration of mid-latitude weather systems is a subtle phenomenon. Some insight into it was gained by Charney (1947) and Eady (1949) who investigated the stability of baroclinic zonal flows to waves of small amplitude growing without changing shape (i.e. of normal mode form), a problem which contains some of the essential physics of the phenomenon in a form which is amenable to mathematical analysis. Later Charney & Stern (1962) and Pedlosky (1964) developed the quasi-geostrophic equations which provide the most convenient mathematical framework for the analytical study of the initial growth of cyclones. According to these equations (see e.g. Pedlosky 1982*a*) the fluid motions are governed by the boundary conditions and the conservation of the quasi-geostrophic potential vorticity q following the geostrophic motion:

$$q_t + J(\psi, q) = 0, \tag{1.1}$$

where

$$q = f + \psi_{xx} + \psi_{yy} + (\psi_z/B)_z. \tag{1.2}$$

Here ψ is the stream function of the geostrophic velocity, subscripts denote partial

derivatives and $J(a,b) = a_x b_y - a_y b_x$ is the Jacobian derivative. Variables have been non-dimensionalized in the standard manner and B, the Burger number, is given by

$$B = N^2 H^2 / f^2 L^2, \tag{1.3}$$

where f is the Coriolis parameter, N the Brunt–Väisälä frequency, and H the vertical and L the horizontal lengthscales used in the non-dimensionalization.

Provided the boundary conditions are inviscid, any steady zonal flow $U(y,z)$ is an exact solution of (1.1) and the evolution of a perturbation ψ' to U is governed by

$$q'_t + Uq'_x + Q_y \psi'_x + J(\psi', q') = 0, \tag{1.4}$$

where Q_y denotes the lateral gradient of the potential vorticity of the basic zonal flow and q' the potential vorticity of the perturbation. The stability of $U(y,z)$ to very small wave-like perturbations of constant shape

$$\psi' = \mathrm{Re}\{\rho(y,z)\exp[\mathrm{i}k(x-ct)]\} \tag{1.5}$$

is hence determined by the well known equation

$$(U-c)q' + Q_y \psi' = 0 \tag{1.6}$$

and its boundary conditions.

Under inviscid boundary conditions the Burger number is the only non-dimensional combination of the imposed conditions on which the solutions of equations (1.1) and (1.6) depend. The evolution governed by (1.1) of waves growing from small amplitude is most easily studied at Burger numbers close to a value, B_0 say, at which there is a neutrally stable wave with stream function ψ_S and real phase speed c_S. The initial growth rate of such waves and the amplitude to which they grow then tends to be small. Consequently the advection of the wave by the zonal flow dominates that by the wave itself in much of the flow. Where this is the case the stream function can usefully be expressed as a summation,

$$\psi' = \sum_{n=1} \delta^n \psi_n, \tag{1.7}$$

in which δ is $B_0 - B$ raised to a suitable (positive) power (Pedlosky 1970; Drazin 1970). The equations governing the wave's evolution can be reduced to a series of forced linear problems

$$(U-c)q_n + Q_y \psi_n = R_n \tag{1.8}$$

(cf. (1.6)) in which R_n is an expression which includes only terms ψ_m and q_m with $m < n$.

Close to B_0 the stream function ψ' of the growing wave is dominated by the stream function ψ_S of the neutral mode itself. The (nonlinear) self-interaction of the slowly growing wave $J(\mathrm{Re}\,\psi', \mathrm{Re}\,q')$, is dominated by

$$J(\mathrm{Re}\,\psi_S, \mathrm{Re}\,q') = -J(\mathrm{Re}\,\psi_S, \mathrm{Re}\{Q_y \psi_S/(U-c)\}) \tag{1.9a}$$

$$= -\mathrm{Re}\,\psi_{Sx}\,\mathrm{Re}\{\psi_S\,\partial/\partial y(Q_y/(U-c))\} + \frac{Q_y c_i}{|U-c|^2} J(\mathrm{Re}\,\psi_S, \mathrm{Im}\,\psi_S) \tag{1.9b}$$

unless (1.9b) is identically zero. The first equality above follows from (1.6) and the second from the definition of the Jacobian. The discussion of this equation in the next three paragraphs contains the main points of the paper.

The first of the two terms on the right-hand side of (1.9b) is identically zero for waves on laterally uniform flows $U(z)$. For most laterally sheared zonal flows $U(y,z)$,

however, $\partial/\partial y\{Q_y/(U-c)\}$ is not identically zero; contours of the stream function and the potential vorticity (p.v.) field of the neutral mode do not coincide and the neutral mode advects its own p.v. field. The second term on the right-hand side of (1.9*b*) is also identically zero for neutral modes subject to inviscid boundary conditions on laterally uniform flows $U(z)$ which increase monotonically with z ($U_z > 0$), for such neutral modes may be taken to be purely real-valued. Thus the dominant nonlinear interaction for inviscid waves depends significantly on the lateral shear of the zonal flow.

Neutral modes subject to Ekman pumping on laterally uniform flows have vertical phase shifts and complex-valued stream functions. Hence the second term on the right-hand side of (1.9*b*) can be non-zero for these modes and represents their dominant nonlinear interaction. It is doubtful, however, that diffusive fluxes in the interior can be consistently neglected for such waves, particularly since Q_y need not be zero at their steering levels. The evolution of waves which are subject to Ekman pumping is not considered in detail below for this reason.

For inviscid waves on a laterally sheared flow, the ratio of the second to the first terms on the right-hand side of (1.9*b*) is of order $c_i \operatorname{Re}\psi_S/\{|U-c|\operatorname{Im}\psi_S\}$. This ratio will always be smaller than or of order 1, so in comparisons with other terms one can limit attention to the first of the two terms on the right-hand side of (1.9*b*). Close to the surface on which U is equal to c_S, which will be referred to as the steering level (despite the fact that it may not be flat), $q'_t + Uq'_x \approx (U-c_S)q'_x$ is small for a slowly growing wave. The nonlinear advection thus dominates the growth rate and linear advection of q near the steering level. From (1.4) and (1.9) it is clear that this is true whether $Q_y/(U-c_S)$ is bounded at the steering level or not. The self-advection of the wave is of the same order of magnitude as the advection by the zonal flow within a region of depth directly proportional to the amplitude of the wave. Within this region, in a time which is inversely proportional to the amplitude of the wave's stream function, many zonal harmonics of the wave's potential vorticity field are excited to amplitudes of the same order of magnitude as that of the potential vorticity of the fundamental. Outside this layer, the self-advection generates only a zonal flow and the second harmonic of the wave ($\sin 2kx$) at an amplitude comparable with the square of the amplitude, A, of the fundamental wave (i.e. of $O(A^2)$). Advection of these by the fundamental produces corrections to the fundamental only of $O(A^3)$.

In order to show that the evolution of the wave as a whole is determined by the advection within the (narrow) critical layer rather than in the bulk of the interior or at the boundaries, the boundary conditions must be considered. We assume that the fluid is confined within horizontal boundaries at $z = -\frac{1}{2}, \frac{1}{2}$ and vertical boundaries at $y = 0$, 1 through which there is no normal motion. When combined with the thermodynamic equation and the Ekman pumping formula the absence of vertical velocity at the horizontal boundaries yields

$$\psi_{zt} + J(\psi, \psi_z) = \pm\epsilon(\psi_{xx} + \psi_{yy}) \quad \text{at} \quad z = \pm\tfrac{1}{2}. \tag{1.10}$$

The precise value of the Ekman pumping parameter is not important here. In the presence of Ekman pumping steady zonal flows with lateral variation generally do not satisfy this condition. For flows that do (e.g. any flow in the absence of Ekman pumping) analysis corresponding to (1.4)–(1.8) yields

$$(U-c_S)\psi_{nz} - U_z\psi_n \pm i\epsilon(\psi_{nxx} + \psi_{nyy}) = S_n \tag{1.11}$$

where S_n is the counterpart of R_n in (1.8).

Provided the steering level is not near the boundaries the main self-interaction of the growing wave there is

$$J(\mathrm{Re}\,\psi_S, \mathrm{Re}\,\psi_{Sz}) = J\left(\mathrm{Re}\,\psi_S, \frac{U_z}{U-c_S}\mathrm{Re}\,\psi_S \pm \frac{\epsilon}{U-c_S}\mathrm{Im}\,\nabla_h^2\psi_S\right)$$

$$= \mathrm{Re}\,\psi_S\,\mathrm{Re}\,\psi_{Sx}\frac{\partial}{\partial y}\left\{\frac{U_z}{U-c_S}\right\} \pm \epsilon J\left(\mathrm{Re}\,\psi_S, \mathrm{Im}\left\{\frac{\nabla_h^2\psi_S}{U-c_S}\right\}\right). \quad (1.12)$$

For laterally uniform flows the first term on the right-hand side of (1.12) is again identically zero and when Ekman pumping is present the vertical variations in the azimuthal phase of the wave, sustaining it against spin-down, give rise to the dominant nonlinear interactions, either at the endwalls ((1.12) and Drazin 1972) or in the interior (see (1.9)). For the more general case of a laterally sheared zonal flow, providing the steering level is confined to the flow interior so that zonal advection dominates, the (self-induced) boundary forcing generates only the second harmonic of the wave and a correction to the axisymmetric flow at amplitudes of $O(A^2)$. No self-induced forcing arises at the sidewalls.

Outside the critical layer, the interior equations (1.8) can be interpreted as formulae for the vertical derivative of ψ_z' whose values at the upper and lower boundaries are constrained by (1.11). The influence of the critical layer on the flow outside it is determined by the jump in ψ_z' across it. Within the critical layer q' is at least of $O(A)$ and variation of the horizontal advection of q' with height will ensure that the stretching term $(\psi_z'/B)_z$ is of the same order as q'. The jump in the fundamental wave's values of ψ_z' across a critical layer whose depth is of $O(A)$ is hence at least of $O(A^2)$. By comparison the nonlinear thermal advection at the boundaries (given by (1.12)) can only affect the fundamental wave at $O(A^3)$ and the advection of potential vorticity in the bulk of the interior similarly affects the difference between the values of the fundamental of ψ_z' at each boundary only at $O(A^3)$.

We conclude from the above discussion that the arrest of the growth of inviscid waves growing from small amplitude on laterally sheared baroclinic flows is qualitatively different from that on laterally uniform flows and that the evolution on laterally uniform flows is not structurally stable (i.e. it is not robust to the introduction of small lateral variations in the zonal flow). On the laterally sheared flow the lateral structure of the neutral wave is complicated enough for it to advect its own potential vorticity field (see (1.9)). This advection is at least comparable with that by the zonal flow within a layer centred on the neutral mode's steering level whose (non-dimensional) depth is of the same order as the amplitude of the wave. The fully nonlinear advection within this narrow layer has a larger effect on the fundamental wave than the nonlinear advection at the boundaries or in the rest of the interior and is hence the first to change the linear growth rate of a disturbance growing from small amplitude.

Sections 2 and 3 present detailed calculations illustrating this evolution on an f-plane for the flow

$$U = \tfrac{1}{2}(1-a_S+a_S\sin\pi y)\sin\pi z, \quad (1.13)$$

which supports neutral normal modes of the form

$$\psi_S = \rho_S(y)\cos kx, \quad c_S = 0. \quad (1.14)$$

The calculations are particularly straightforward for this case because $Q_y/(U-c_S)$ is

bounded at the steering level and the steering level is horizontal, lying on the plane $z = 0$. In §2 the domain is divided into a region surrounding the steering level and two outer regions and the solutions in each region matched together. The resulting equation describing the evolution of the wave amplitude and of the potential vorticity in the critical layer is similar to that obtained by Warn & Gauthier (1989), but is difficult to solve analytically. Numerical solutions are presented in §3.

Various features and deficiencies of these solutions and their relationship to other recent work are discussed in §4 whilst §5 contains a discussion of the relevance of the solutions to the flows obtained near the upper axisymmetric transition in the differently heated rotating annulus experiments (Hide & Mason 1975). This paper developed from attempts to understand these flows, and joint laboratory and numerical investigations of them appear to be the most promising approach to determining whether the processes described here are important in real fluids. Concluding remarks are made in §6.

2. Analysis of a nonlinear baroclinic critical layer

2.1. *Problem definition*

The quasi-geostrophic equations for an f-plane will be assumed to govern the motion:

$$Bq_t + J(\psi, Bq) = 0, \quad -\tfrac{1}{2} \leqslant z \leqslant \tfrac{1}{2}, \tag{2.1}$$

$$Bq = B(f + \nabla_{\mathrm{h}}^2 \psi) + \psi_{zz}, \tag{2.2}$$

$$\psi_{zt} + J(\psi, \psi_z) = 0 \quad \text{on} \quad z = \pm\tfrac{1}{2}, \tag{2.3}$$

$$\psi_x = 0 \quad \text{and} \quad \Psi_{yt} = 0 \quad \text{on} \quad y = 0, 1. \tag{2.4}$$

Equation (2.1) represents conservation of the quasi-geostrophic potential vorticity (2.2) following the geostrophic motion. Equation (2.3) represents conservation of potential temperature at the horizontal boundaries where the vertical velocity vanishes in the absence of Ekman pumping. No normal flow and energy-conserving conditions on the zonal mean stream function Ψ are applied at the side boundaries (2.4). The stratification is taken to be independent of height and the channel to be periodic in x with non-dimensional repeat length l_{S}. The zonal flow is assumed to be an internal baroclinic jet (Charney & Stern 1962) of the form

$$U = \tfrac{1}{2} \sin \pi z \, (1 - a_{\mathrm{S}} + a_{\mathrm{S}} \sin \pi y). \tag{2.5}$$

This flow is studied at a Burger number slightly smaller than that at which there is a neutral mode which advects its own potential vorticity field (see (1.9)). The evolution of the only unstable weakly growing normal mode is traced as it grows from a very small initial amplitude.

The form of the neutral normal mode and the appropriate scalings are summarized first. The outer solutions (i.e. those outside the critical layer) are then developed and the jump conditions across the critical layer established. Presentations of the inner solution and the matching of the inner solution with the jump in the outer thermal field across the critical layer follow. Finally formulae are derived for the unstable linear normal mode in the inner and outer regions (which serve as the initial conditions). The key formulae are summarized at the end of the section.

The potential vorticity fields of the inner and outer solutions will be denoted by

p and q respectively and the inner and outer stream functions by ϕ and ψ. P, Q, Φ and Ψ denote the corresponding zonal mean fields.

2.2. *Neutral mode solution*

BQ_y/U is well defined for (2.5) and independent of height:

$$\frac{BQ_y}{U} = \pi^2 + \frac{B\pi^2 a_S \sin \pi y}{1 - a_S + a_S \sin \pi y}. \tag{2.6}$$

Direct substitution in (2.1)–(2.4) shows that

$$\psi_S = \rho_S(y) \cos r\pi x \quad \text{with} \quad r = 2/l_S \tag{2.7}$$

is a stationary solution ($c_S = 0$) of the quasi-geostrophic equations linearized about the zonal flow (2.5) when ρ_S is the gravest mode solution of

$$\left.\begin{aligned} \rho_{yy} + \frac{\pi^2 a_S \sin \pi y}{1 - a_S + a_S \sin \pi y}\rho + \lambda\rho = 0, \quad 0 \leqslant y \leqslant 1 \\ \rho = 0 \quad \text{on} \quad y = 0, 1, \end{aligned}\right\} \tag{2.8}$$

and the Burger number, B, is related to the gravest mode's eigenvalue, λ_S, by

$$B = \frac{\pi^2}{\lambda_S + r^2\pi^2} = B_0. \tag{2.9}$$

This neutral mode solution is clearly non-singular and independent of height. Bell & White (1988) (and Bell 1989) show that the normal mode which springs from this neutral one as B is reduced is the only unstable normal mode at values of B just smaller than B_0.

2.3. *Scaling considerations*

The Burger number is assumed to be just less than B_0:

$$B = B_0 - \Delta B. \tag{2.10}$$

As shown by Bell & White (1988) (and in Appendix B) the normal mode growth rate is then of $O(\Delta B)$. So we introduce an appropriate slow time τ:

$$\tau = \Delta B t. \tag{2.11}$$

Harmonics and nonlinear corrections to the dominant wave mode are generated by the neutral mode's self-advection at a rate of $O(A^2)$, A being the wave amplitude. So the nonlinear advection can combat the linear growth if

$$A = \Delta B\, a(\tau), \tag{2.12}$$

$a(\tau)$ being of $O(1)$ when linear growth and nonlinear advection become comparable. Since within the critical layer the zonal velocity U of (2.5) is of the order $\frac{1}{2}\pi z$, the critical layer has a depth of $O(\Delta B)$ (for $z \gg \Delta B$ zonal flow advection dominates). So the stretched vertical ordinate ζ,

$$z = \Delta B\, \zeta, \tag{2.13}$$

will be used within the critical layer. The inner solution has domain $-\infty < \zeta < +\infty$ and for $\zeta \to \pm\infty$ must match the outer solutions for $z \to 0^{\pm}$.

2.4. *Outer solutions*

Two outer solutions are required; one above and one below the critical layer. The equations governing the two are very similar and for the most part they will not be painstakingly distinguished. We pose the perturbation expansion for the stream function suggested by (2.12)

$$\psi = \Psi_0 + \Delta B\,\psi_1 + \Delta B^2\psi_2 + \ldots \tag{2.14}$$

in which Ψ_0 is the stream function of the zonal flow (2.5). Substituting into (2.1) times B_0/B and (2.3), and using (2.10) one obtains at $O(\Delta B)$:

$$\left.\begin{aligned} \mathrm{M}_0\psi_{1x} \equiv (B_0\nabla_{\mathrm{h}}^2 + \partial^2/\partial z^2)\,\psi_{1x} + (BQ_y/U)_{B=B_0}\psi_{1x} = 0, \\ \psi_{1zx} = 0 \quad \text{on} \quad z = \pm\tfrac{1}{2}. \end{aligned}\right\} \tag{2.15}$$

So the outer solution to first order is proportional to the gravest mode solution:

$$\psi_1 = \{a(\tau)\cos r\pi x + b(\tau)\sin r\pi x\}\,\rho_{\mathrm{S}}(y). \tag{2.16}$$

Strictly speaking the most general outer solutions should be matched across the critical layer to reach this conclusion; but the depth-independent solution (2.16) does satisfy the inner equations at lowest order as will become apparent. An undetermined x-independent perturbation should also be retained at this point but examination of the problem at the next order ((2.17) below) shows that it is not excited at this order.

At $O(\Delta B^2)$ (2.1) times $B_0/(BU)$ and (2.2) yield

$$\mathrm{M}_0\psi_{2x} = -B_0/U\,\nabla_{\mathrm{h}}^2\psi_{1\tau} - J(\psi_1, B_0\nabla_{\mathrm{h}}^2\psi_1)/U + U_{zz}\psi_{1x}/(B_0U), \tag{2.17}$$

$$\psi_{2zx} = 0 \quad \text{on} \quad z = \pm\tfrac{1}{2}. \tag{2.18}$$

The left-hand side of (2.17) involves an elliptic operator (defined in (2.15)) on ψ_{2x} and the right-hand side terms $-B_0 q_{1\tau}/U$ and $-J(\psi_1, B_0 q_1)/U$ which are singular at $z = 0$ on the edges of the two domains. The forcing terms on the right-hand side of (2.17) do not induce any axisymmetric motions as anticipated in (2.16). Equations (2.17) and (2.18) become a well-defined problem if jump conditions on ψ_2 and ψ_{2z} across $z = 0$ are specified:

$$[\psi_2]_{0^-}^{0^+} = H(x,y); \quad [\psi_{2z}]_{0^-}^{0^+} = I(x,y). \tag{2.19}$$

$H(x,y)$ and $I(x,y)$ are understood to depend on the inner solution.

As shown in Appendix A, (2.17)–(2.19) have solutions provided

$$\left[\iint \rho_{\mathrm{S}}(y)\exp(\mathrm{i}r\pi x)\,\psi_{2z}\,\mathrm{d}x\,\mathrm{d}y\right]_{-z}^{z} \to \frac{\pi^2}{B_0}\iint \rho_{\mathrm{S}}(y)\exp(\mathrm{i}r\pi x)\,\psi_1\,\mathrm{d}x\,\mathrm{d}y \quad \text{as} \quad z\downarrow 0. \tag{2.20}$$

This (Fredholm type) condition ensures that $I(x,y)$ does not resonantly force (2.17) by projecting onto the unforced neutral solution.

2.5. *Inner solution*

From (2.2) and (2.13), the potential vorticity in the critical layer, p, is related to the stream function, ϕ, by

$$Bp = Bf + B\nabla_{\mathrm{h}}^2\phi + \frac{1}{\Delta B^2}\phi_{\zeta\zeta}. \tag{2.21}$$

The conservation of potential vorticity, (2.1), is expressed by

$$\Delta B\{Bp_\tau + J(\phi, Bp\} = 0. \tag{2.22}$$

We pose a series expansion for ϕ in powers of ΔB:

$$\phi = \Delta B\,\phi_1 + \Delta B^2\phi_2 + \Delta B^3\phi_3 + \ldots. \tag{2.23}$$

For $\zeta \to \pm\infty$, ϕ must match to the outer solution with $z \to 0^{\pm}$ which is given to $O(\Delta B)$ by

$$\psi_{\text{out}} = \Delta B\{\tfrac{1}{2}\pi\zeta - \tfrac{1}{12}\Delta B^2(\pi\zeta)^3 + O(\Delta B^4)\}\{-(1-a_{\text{S}})\,y + a_{\text{S}}/\pi\cos\pi y\} + \Delta B(a(\tau)\cos r\pi x + b(\tau)\sin r\pi x)\,\rho_{\text{S}}(y) + O(\Delta B^2). \tag{2.24}$$

The terms of $O(\Delta B^3)$ in (2.24) describe the initial zonal mean flow to $O(\Delta B^3)$. They are included for reference in the derivation of (2.31) below.

At $O(1)$ (2.22) is

$$\phi_{1\zeta\zeta\tau} + J(\phi_1, \phi_{1\zeta\zeta}) = 0. \tag{2.25}$$

A (barotropic wave) solution which matches to the outer one is

$$\phi_1 = -\tfrac{1}{2}\pi\zeta\left\{(1-a_{\text{S}})\,y - \frac{a_{\text{S}}}{\pi}\cos\pi y\right\} + \rho_{\text{S}}(y)\,(a(\tau)\cos r\pi x + b(\tau)\sin r\pi x). \tag{2.26}$$

The mean flow in the outer solution is time independent so $\Phi_{1\tau} = 0$.

At $O(\Delta B)$ (2.22) is

$$\phi_{2\zeta\zeta\tau} + J(\phi_1, \phi_{2\zeta\zeta}) = 0. \tag{2.27}$$

The partial solution

$$\phi_2 = \Phi_2(y,\zeta) + \sum_{k,l}(c^{(k,l)}\cos rk\pi x + d^{(k,l)}\sin rk\pi x)\,\rho^{(k,l)}(y), \tag{2.28}$$

in which the $\rho^{(k,l)}(y)$ are eigenfunctions of M_0 (see (2.15) and Appendix A), is adequate. Solutions with $\phi_{2\zeta\zeta}$ non-zero would require potential vorticity gradients of $O(1)$ which cannot develop for ζ of $O(1)$ since p is conserved by the horizontal geostrophic motion. (Such solutions are probably important in the development of flows with singular critical levels.) Wave solutions directly proportional to ζ are not required because the $O(\Delta B)$ outer streamfunction (2.16) is barotropic (i.e. $\psi'_z = 0$).

At $O(\Delta B^2)$, the highest-order considered here, (2.22) is

$$p_{1\tau} + J(\phi_1, p_1) = 0, \tag{2.29}$$

where

$$Bp_1 = B_0\nabla_{\text{h}}^2\phi_1 + \phi_{3\zeta\zeta}. \tag{2.30}$$

Equations (2.29) and (2.30) assert that the $O(\Delta B)$ potential vorticity, p_1, is conserved following the $O(\Delta B)$ geostrophic motion. Using (2.24) one finds that the zonal flow by itself initially has

$$BP_1 = \tfrac{1}{2}\pi^3\zeta\left\{(1-a_{\text{S}})\,y - (1+B_0)\frac{a_{\text{S}}}{\pi}\cos\pi y\right\}. \tag{2.31}$$

The inviscid boundary conditions (2.4) imply that $\phi'_3 = 0$ on $y = 0, 1$ and (2.26) with (2.8) implies that $\phi'_{1yy} = 0$ on $y = 0, 1$ so

$$p'_1 = 0 \quad \text{on} \quad y = 0, 1. \tag{2.32}$$

Furthermore $\Phi_{1y\tau} = 0$ and $\Phi_{3y\tau} = 0$ on $y = 0, 1$. For a pure wave perturbation $\Phi_3 = 0$ at time $\tau = 0$, so using (2.31)

$$BP_{1y} = \tfrac{1}{2}\pi^3\zeta(1-a_{\text{S}}) \quad \text{on} \quad y = 0, 1. \tag{2.33}$$

2.6. *Matching condition*

For the inner, ϕ, and outer, ψ, solutions to match, they and their derivatives must agree over an intermediate range of depths $z_a < z_0 < z_b$ in which $z_0/\Delta B \to \infty$ and $z_0 \to 0$ as $\Delta B \to 0$. Within this range of depths we thus require

$$[\psi'_z]_{z=-z_0}^{z=+z_0} = [\phi'_\zeta/\Delta B]_{\zeta=-z_0/\Delta B}^{\zeta=z_0/\Delta B} \quad \text{as} \quad \Delta B \to 0. \tag{2.34}$$

For the solutions presented above, to $O(\Delta B^2)$ (2.34) is

$$\Delta B^2 [\psi'_{2z}]_{z=0^-}^{z=0^+} = \Delta B^2 \int_{\zeta=-\infty}^{\zeta=+\infty} \phi'_{3\zeta\zeta}\, \mathrm{d}\zeta. \tag{2.35}$$

Using (2.35), the solvability condition (2.20) can be expressed as

$$\iiint_{-\infty}^{+\infty} \rho_S \exp(\mathrm{i}r\pi x)\, \phi_{3\zeta\zeta}\, \mathrm{d}\zeta\, \mathrm{d}x\, \mathrm{d}y = \frac{\pi^2}{B_0} \iint \rho_S \exp(\mathrm{i}r\pi x)\, \psi_1\, \mathrm{d}x\, \mathrm{d}y. \tag{2.36}$$

2.7. *Initial conditions*

An appropriate initial condition for the perturbation stream function is that of the linearly unstable normal mode (though see Warn & Gauthier 1989, §2(ii)). As shown in Appendix B the normal mode with an initial outer stream function of small amplitude γ,

$$\phi'_1 = \gamma \cos(r\pi x)\, \rho_S(y), \tag{2.37}$$

has accompanying vertical variation

$$\phi'_{3\zeta\zeta} = \frac{\gamma B_0 (Q_y/U)\, \rho_S}{|\tilde{U}-c|^2} \{|c|^2 \cos(r\pi x) + \tilde{U}|c| \sin(r\pi x)\} \tag{2.38}$$

in the critical layer. In (2.38)

$$\tilde{U} = \tfrac{1}{2}\Delta B \pi \zeta (1 - a_S + a_S \sin \pi y) \quad \text{and} \quad c = \frac{\mathrm{i}\Delta B T}{2B_0^2} \tag{2.39}$$

with

$$T = \frac{\int \pi^2 \rho_S^2\, \mathrm{d}y}{\int \rho_S^2 (Q_y/U)(1 - a_S + a_S \sin \pi y)^{-1}\, \mathrm{d}y}. \tag{2.40}$$

2.8. *Summary*

The above analysis treats the development of a wave which starts as a slowly growing normal mode disturbance of small amplitude on a baroclinic zonal flow which has $Q_y = U = 0$ on $z = 0$ (see (2.5)). It is set at a Burger number, $B_0 - \Delta B$, where this wave is the only linearly unstable normal mode. The wave is governed by its evolution in a critical layer with a depth of $O(\Delta B)$ and grows to an amplitude of $O(\Delta B)$. Its stream function to $O(\Delta B)$ is barotropic both inside and outside the critical layer (see (2.26) and (2.16)) and has the same spatial form as the neutral normal mode (2.7). The $O(\Delta B)$ potential vorticity within the critical layer, p_1 as defined by (2.30), is conserved following the $O(\Delta B)$ geostrophic motion (2.29). Boundary conditions on p_1 are provided by (2.32) and (2.33) and the amplitudes $a(\tau)$ and $b(\tau)$ of the $O(\Delta B)$ wave stream function are determined by the constraint (2.36) which ensures that the jump in the thermal field across the critical layer (resulting from potential vorticity

advection within it) does not resonantly force the neutral normal mode outside the critical layer.

3. Numerical solutions

3.1. *Method*

Numerical solutions for the potential vorticity in the inner region have been obtained using a gridpoint model with variable vertical and horizontal resolution. On the *IZ*th level a uniform grid is employed with *IXP*(*IZ*) points along-stream and *IYP*(*IZ*) points within the channel across-stream. The cross-stream gridpoints straddle the boundaries $y = 0, 1$ and conditions (2.32) and (2.33) are applied using second-order-accurate formulae. Forward steps of (2.29) are performed by the leapfrog method with the source function $J(\phi_1, p_1)$ evaluated according to Arakawa's energy and enstrophy conserving formula (Haltiner & Williams 1980). Explicit horizontal diffusion is invoked to dampen small scales, so that in place of (2.29) the equation being integrated is

$$p_{1\tau} = -J(\phi_1, p_1) + \nu_a \nabla_h^2 p_1 - \nu_b \nabla_h^4 p_1 \equiv S_1. \tag{3.1}$$

Standard four-point formulae are used for the Laplacian operators and the additional homogeneous boundary condition

$$\nabla_h^2 p_1 = 0 \quad \text{on} \quad y = 0, 1 \tag{3.2}$$

is used when ν_b is non-zero. A very weak Robert filter with coefficient R_f is employed to dampen the computational mode; the resulting error in the source function is

$$\Delta S_1 = p_{1\tau\tau} \Delta\tau^2 R_f, \tag{3.3}$$

$\Delta\tau$ being the timestep. In all integrations the initial forward step is specified to be one eighth of the standard length and Miyakoda's method (Hoskins & Simmons 1975) used to reach the standard step length.

In the experiments reported here, for $-2c_1 < \zeta < 2c_1$ (i.e. close to the steering level) the vertical spacing (*DZ*1) and horizontal spacing are independent of depth and $\zeta = 0$ is chosen to be one of the levels. The numbers of points along- and across-stream in this region are denoted by *IXPTS* and *IYPTS* respectively. In order to obtain an r% relative error in the initial growth rate, the depth of the domain, h, must be great enough that the integral

$$I(h) = \int_{-h}^{+h} \frac{c_1}{(\zeta^2 + c_1^2)} \mathrm{d}\zeta = 2 \arctan(h/c_1) \tag{3.4}$$

is within r% of $I(h = \infty)$. For a 5% error in $I(h)$ we need $h > 16c_1$. Manipulation of standard formulae bounding the error in evaluations of I by the trapezoidal rule (Kreyszig 1982) suggests that the contribution to the error is (roughly) the same from each layer at large values of $|\zeta|$ if the level spacing is proportional to $|\zeta|^{\frac{4}{3}}$. The level spacing is specified to grow at this rate for $|\zeta| > 2c_1$.

Since the zonal flow is proportional to ζ, for large values of $|\zeta|$ the zonal flow is very strong. In order to satisfy the CFL stability criterion the horizontal resolution must decrease with $1/|\zeta|$, or the timestep be inversely proportional to the height of the top level. Since good horizontal resolution is only required near the steering level the former option is used and for $|\zeta| > 2c_1$

$$IXP(IZ) = IXPTS/(\tfrac{1}{2}|\zeta|(IZ)/c_1). \tag{3.5}$$

IYP(*IZ*) varies similarly with ζ.

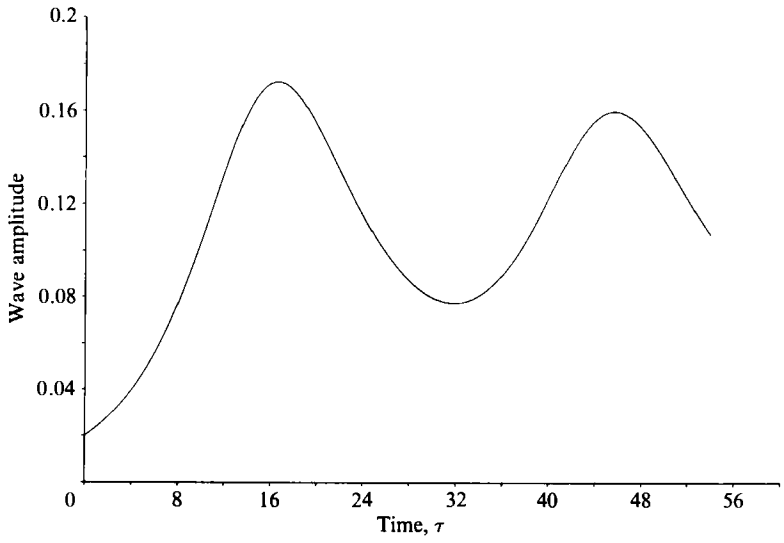

FIGURE 1. The evolution of the amplitude, $a(\tau)$, of the wave (2.16) as a function of the slow time $\tau = \Delta B t$ during experiment A.

Exp.	A	B	C	D	E	F
IXPTS	128	128	128	64	128	128
IYPTS	64	64	64	32	64	64
IZPTS	26	26	22	22	13	26
*DZ*1	0.035	0.035	0.035	0.035	0.07	0.035
Top level	2.64	2.64	1.4	1.4	2.19	2.64
ν_b	3×10^{-8}	3×10^{-9}	3×10^{-8}	3×10^{-8}	3×10^{-8}	0
ν_d	0	0	0	0	0	2×10^{-4}

TABLE 1. The parameter settings used in the numerical experiments described in §3

In order to reduce the computational cost, advantage was taken of symmetries present in the initial conditions and retained by solutions of the governing equations which are derived in detail in Bell (1989). In particular $b(\tau)$ retains its initial value of zero and p_1 below $\zeta = 0$ may be inferred from p_1 above $\zeta = 0$ using

$$p_1(-x+l_S/2, y, -\zeta) = -p_1(x, y, \zeta). \tag{3.6}$$

Finally it is desirable that the initial amplitude of the wave be chosen to ensure that initially p_1 has no closed contours within the critical layer. These form first (as γ is increased) near the sidewall. Comparison of the initial fields of P_{1y} and p'_{1y} shows that $|P_{1y}| > |p'_{1y}|$ and hence there are no closed contours when

$$\gamma|\rho_{Sy}| < c_1 \quad \text{at} \quad y = 0, 1. \tag{3.7}$$

3.2. *Results*

In all the experiments to be presented the zonal flow has $a_S = 0.5$ (see (2.5)) and the channel aspect ratio $l_S = 2\pi$. For these settings the linear growth rate $c_1 \approx 0.175$. Each integration starts from the linear normal mode solution with an initial amplitude $\gamma = 0.02$ (which satisfies (3.7)) at time $\tau = 0$ and proceeds for at least 1800 steps to $\tau = 27$.

In experiment A there are 10 equally spaced levels between $\zeta = 0$ and $\zeta = 0.35 =$

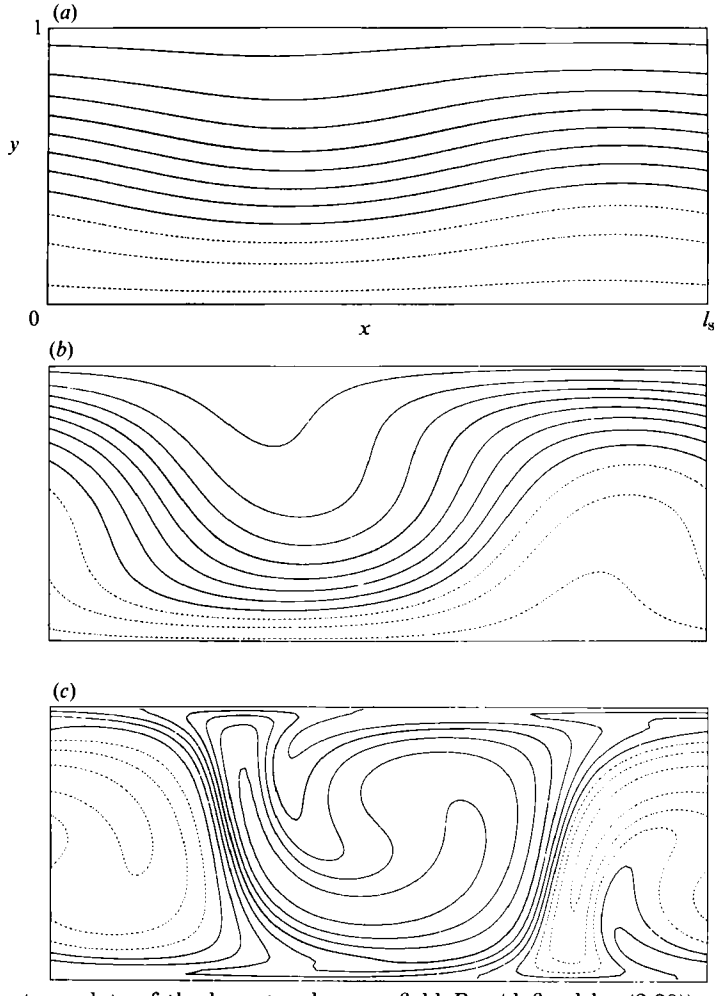

FIGURE 2. Contour plots of the lowest-order p.v. field Bp_1 (defined by (2.30)) on level $\zeta = 0.105$ within the critical layer obtained during experiment A at slow times (*a*) $\tau = 0$, (*b*) $\tau = 9$, (*c*) $\tau = 18$. The contour interval is 0.2 and negative contours are dashed.

$2c_1$, their spacing $DZ1$ being 0.035. On each of these levels there are 128 points along the channel and 64 points across it, i.e. $IXPTS = 128$ and $IYPTS = 64$. There are 26 levels at or above $\zeta = 0$ in all, the highest being at $\zeta = 2.64$. On this level $IXP = 16$ and $IYP = 8$. The domain covered extends to about $\zeta = 2.87$ so the vertical truncation of the domain is expected to introduce a relative error of about 5% in the initial growth rate. In order to simulate the inviscid problem, biharmonic diffusion was employed with weak dissipation coefficients: $\nu_d = 0$, $\nu_b = 3 \times 10^{-8}$.

The parameters detailed above for experiment A are summarized for all the experiments in table 1. The timestep used for all experiments is $\Delta\tau = 0.0015$. This comfortably satisfies the CFL condition on all levels. Solutions were found to be insensitive to the Robert parameter R_f provided it lay between 10^{-4} and 10^{-2}. In all experiments presented, $R_f = 10^{-3}$.

The amplitude $a(\tau)$ of the stream function as a function of time in experiment A is plotted in figure 1. It reaches a first maximum near $\tau = 16$, a minimum near $\tau = 32$ and a second maximum near $\tau = 44$. Clearly the integration is too short to

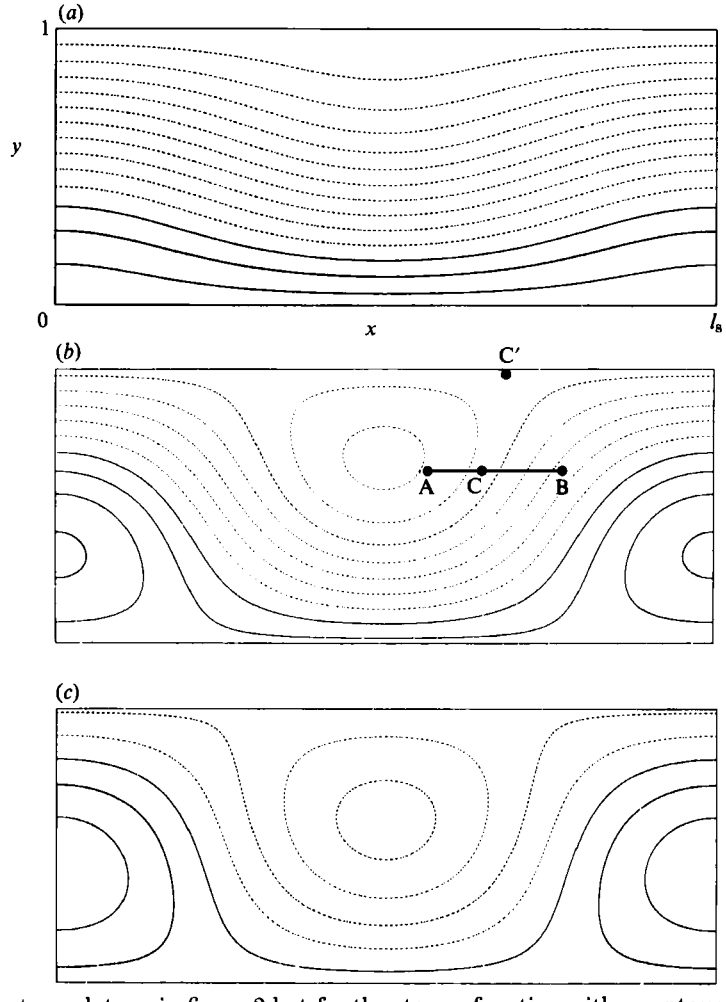

FIGURE 3. Contour plots as in figure 2 but for the stream function with a contour interval of 0.02. The evolution of the line segment ACB is discussed in §4. C′ denotes a stagnation point of the flow.

determine whether the flow will reach a wave-like steady state or vacillate indefinitely. Figure 2 depicts the potential vorticity field multiplied by B, Bp_1, on level $\zeta = 0.105$ at times $\tau = 0$, 9 and 18. The stream function on the same level at these times is presented in figure 3, and Bp_1 at times $\tau = 27$, 36 and 54 in figure 4. In the latter figure Bp_1 is clearly assuming fine structure and large gradients with sharp corners in the contours of constant Bp_1. Irreversible deformation of the p.v. contours (McIntyre & Palmer 1985) due to advection by the stream function is certainly occurring within non-dimensional depths of the order of ΔBc_1 of the steering level. Figure 5 displays the solution on level $\zeta = 0.21$ at times $\tau = 0$, 18 and 27 where the distortion of the potential vorticity field is less intense. At the highest level in the simulation (not shown) Bp_1 is dominated by the zonal flow and the wave's perturbation to the contours barely perceptible. The qualitative nature of the solutions is discussed further at the start of the next section.

Experiments B–E were performed to investigate the sensitivity of experiment A to various parameters. Figure 6 presents the fields of Bp_1 obtained in experiments B, C

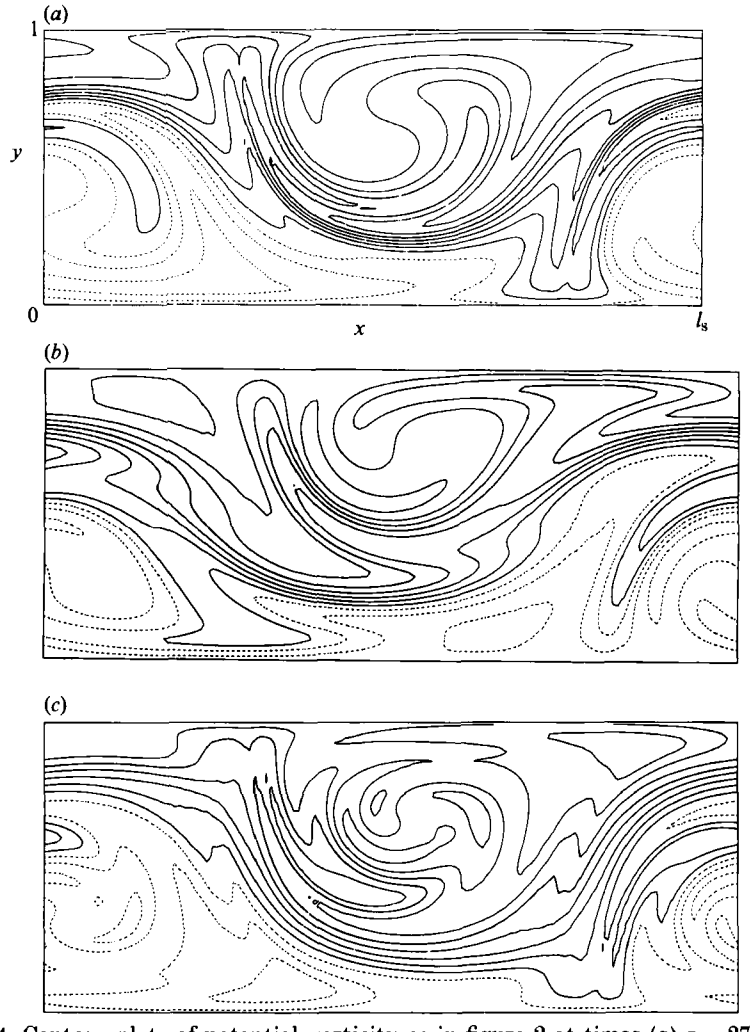

FIGURE 4. Contour plots of potential vorticity as in figure 2 at times (*a*) $\tau = 27$, (*b*) $\tau = 36$, (*c*) $\tau = 54$.

and D at time $\tau = 27$ on level $\zeta = 0.105$ which may be compared with that for A (figure 4*a*). Table 2 provides the values of the amplitude $a(\tau)$ obtained in each experiment at times $\tau = 9$, 18 and 27.

Experiment B is a repeat of A with the diffusive parameter reduced by a factor of 10. At this setting diffusion cannot quite control the grid-scale roughness which develops from corners in the Bp_1 contours (see figure 6*a*). The amplitudes obtained in A and B nevertheless agree to within 1% for $\tau < 18$ and 3% at $\tau = 27$. In areas with strong gradients of Bp_1 the contours are noticeably tighter in experiment B then A. The lack of tightening of contours in experiment A after $\tau = 27$ (figure 4) may thus be due to the diffusion used.

Experiment C is a repeat of A except that the top four levels used in A are not present in experiment C. In C, $I(h)$ is evaluated with $h = 1.60$. The ratio of the amplitudes obtained during A and C at $\tau = 9$ is comparable with the ratio of their values for $I(h)$. Comparison of figures 6(*a*) and 6(*b*) shows that the advection is slightly further advanced in experiment C in which the wave amplitude is generally

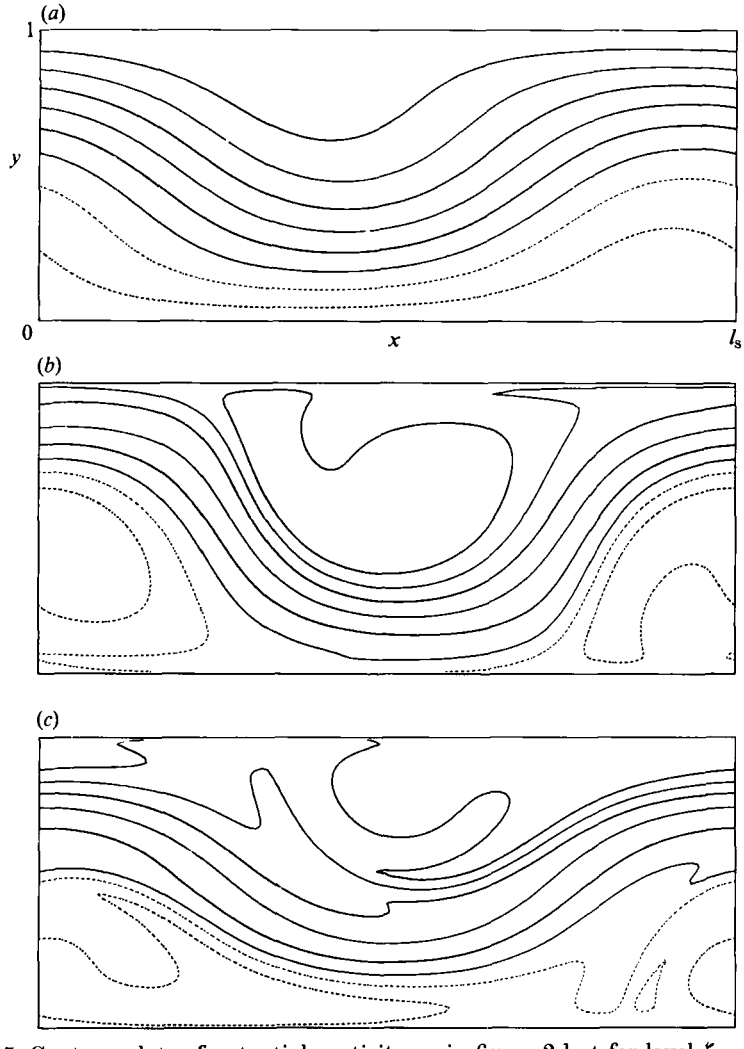

FIGURE 5. Contour plots of potential vorticity as in figure 2 but for level $\zeta = 0.21$ with a contour interval of 0.5.

larger (for $\tau < 27$). Experiment D is a repeat of C with the horizontal resolution in each direction halved on every level. On the top level, $\zeta = 1.40$, $IXP = 16$ and $IYP = 8$. The diffusive parameter is too small to control grid-scale roughness fully (compare figures 6*a* and 6*c*) but the amplitudes in experiments C and D agree to within 2% for $\tau < 18$ and within 4% at $\tau = 27$. Finally experiment E is a repeat of A except that the vertical spacing between levels is doubled whilst the top of the domain is almost unaltered ($h = 2.53$). Differences between A and E are very slight (see table 2) and may be accounted for by the slight drop in h between A and E (cf. A and C).

We conclude that the qualitative form of the variation of the amplitude in figure 1 is representative of that for the inviscid problem but that the amplitude at the first maximum is probably about 5% larger than would be obtained in the inviscid case. The potential vorticity fields from run A are also fairly reliable but probably underestimate the strongest gradients when $\tau > 18$.

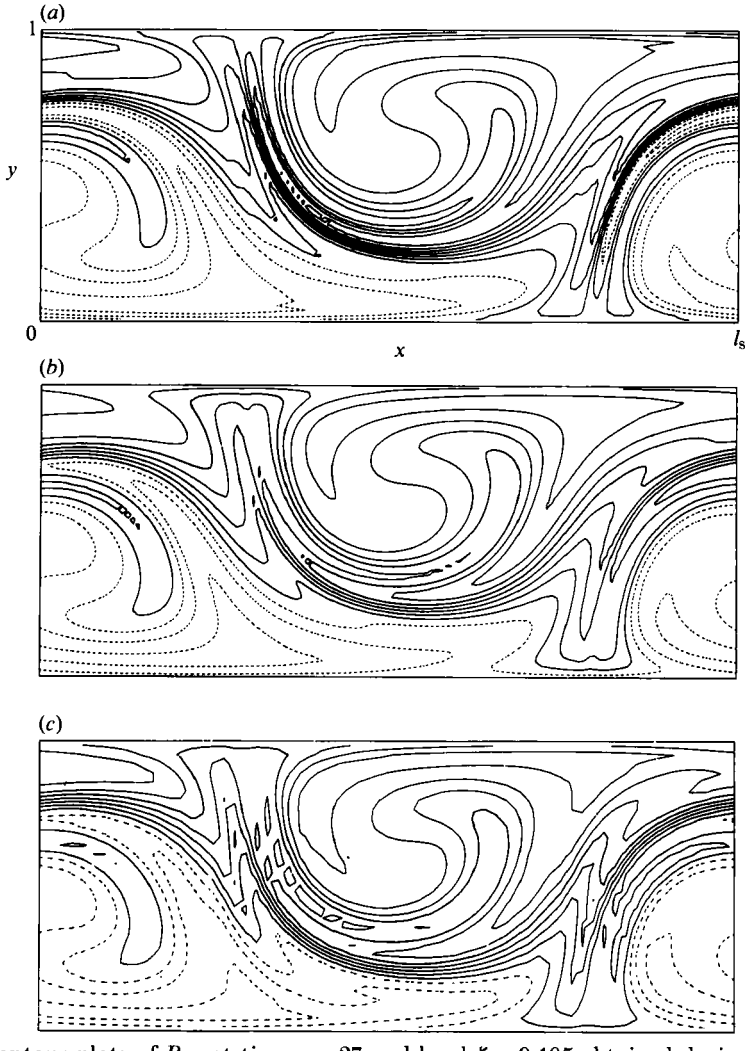

FIGURE 6. Contour plots of Bp_1 at time $\tau = 27$ and level $\zeta = 0.105$ obtained during (*a*) experiment B, (*b*) experiment C, (*c*) experiment D. The corresponding plot for experiment A is figure 4(*a*).

$a(\tau)$	$\tau = 9$	$\tau = 18$	$\tau = 27$
A	0.0905	0.1687	0.0924
B	0.0901	0.1692	0.0956
C	0.0943	0.1739	0.0939
D	0.0922	0.1750	0.0977
E	0.0908	0.1693	0.0925
F	0.0778	0.1238	0.051

TABLE 2. The amplitude of the wave, $a(\tau)$, obtained at three times in each of experiments A–F

A single experiment, F, is presented to illustrate the effect of moderate diffusion on the potential vorticity evolution in the critical layer. F is a repeat of A except that ν_b is set to zero and $\nu_d = 3 \times 10^{-4}$. Figure 7 displays the fields of Bp_1 obtained for experiment F on level $\zeta = 0.105$ at times $\tau = 9$, 18 and 27. Comparison with figure 1,

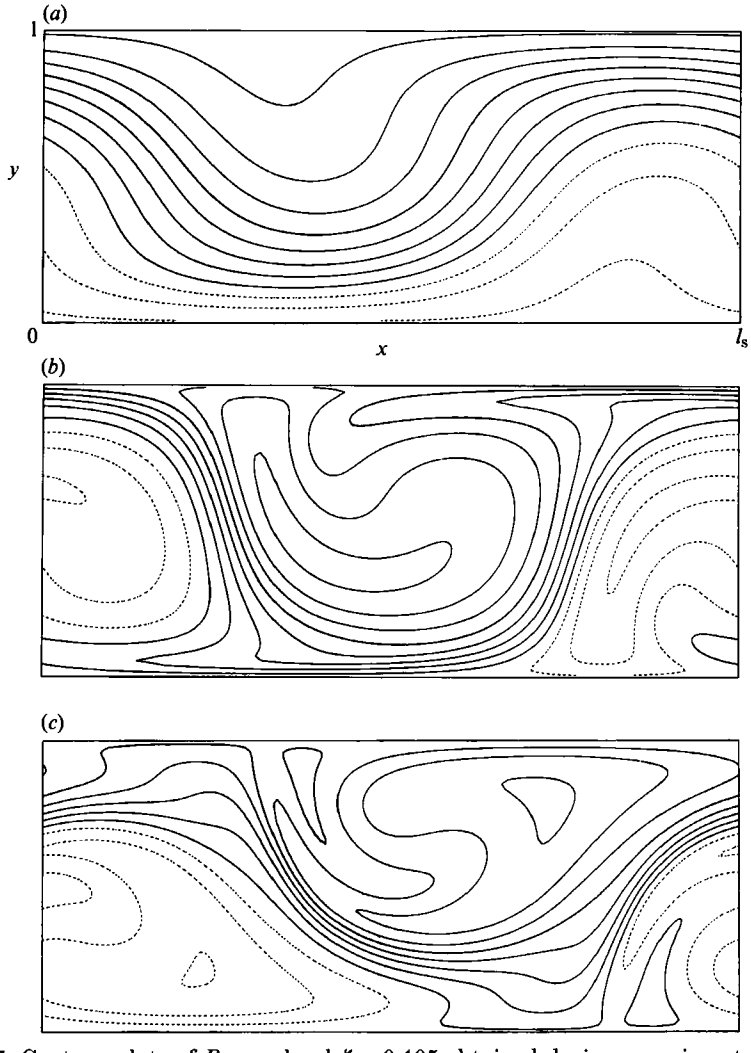

FIGURE 7. Contour plots of Bp_1 on level $\zeta = 0.105$ obtained during experiment F (in which $\nu_d = 2 \times 10^{-4}$) at times (*a*) $\tau = 9$, (*b*) $\tau = 18$, (*c*) $\tau = 27$.

which displays the corresponding fields for experiment A, shows that the distortion of the field of Bp_1 is severely limited by diffusion of this order. From table 2, it is clear that the diffusion also retards the initial growth of the wave, indeed when $\nu_d > 10^{-3}$ the inviscid normal mode analysis on which the work of §2 is based is probably inappropriate.

4. Discussion

4.1. *Qualitative nature of solutions*

The qualitative nature of the evolution of the potential vorticity fields presented in the last section is perhaps most easily grasped by consideration of the advection of a segment such as AB in figure 3 (*b*) by the stream function shown in that figure. Note that AB follows closely an original q-contour (figure 2*a*). Point A is advected about

a closed streamline encircling the centre of the domain whilst B is advected about the other gyre and a point close to C must be advected ever more slowly towards the stagnation point C′ of the flow. After the fluid parcel at A has circled n times around its gyre, the advected segment must spiral (at least) n times around the gyre's centre before connecting to the parcel originally at C, which has moved close to C′.

When the stream function is steady, all parcel trajectories are orbits or fixed points. It is an intrinsic feature of the problem posed in this paper, however, that the shape of the stream function in the critical layer and the location of C′ changes with the amplitude of the wave. Which gyre a parcel passing close to C will circulate next depends on the precise amplitude of the wave. If the amplitude of the wave never attains a steady value, fluid parcels passing close to C will follow chaotic trajectories.

The description given by Rhines & Young (1983) of the (coarse-grain streamwise) homogenization of passively advected tracers by cross-stream shearing provides an alternative view of the evolution of the p.v. fields. The force-like nature of this homogenization, which is directed so as to weaken the zonal flow, is explained in Rhines & Holland (1979, equations 8 and 16).

4.2. *Comparisons with other work*

Maslowe (1986) gives a useful review of nonlinear critical layers in shear flows. The problem that has been studied in most detail is that of a forced barotropic Rossby wave impinging on a critical layer (Stewartson 1978; Warn & Warn 1978). Here the nonlinear advection occurs chiefly within Kelvin's cat's eyes centred on the critical level of the forced wave. More recently, Churlov & Shukhman (1987) have studied the nonlinear development of a wave growing from small amplitude on a slightly supercritical two-dimensional unbounded shear flow. In this problem (see their §9) the critical layer is non-singular and the waves again have the form of cat's eyes in the critical layer. As already noted, Warn & Gauthier's (1989) study of waves on a marginally unstable baroclinic flow is closely related to the present work. The stream functions in their critical layers are of a similar wave-like form to those of this paper (though their shapes are independent of time). The main differences between the papers are that this one concerns a continuously stratified fluid and a laterally sheared zonal flow whilst they consider a two-layer fluid and a laterally uniform zonal flow. Unstable waves on laterally sheared baroclinic flows have been investigated by James (1987) and Feldstein & Held (1989). The barotropic linear shear considered by James gives rise to a strongly sloping steering level but does not affect the p.v. gradient and is thus complementary to that discussed here. Feldstein & Held's numerical study with a two-layer model is again complementary to this one as it focuses on waves growing on one part of a flow and impinging on singular critical layers in other parts.

4.3. *Non-generic aspects of the problem posed*

Two aspects of the problem posed in §2 are rather artificial and 'non-generic'. First, the steering level of the neutral mode is flat. Horizontal advection by the neutral mode consequently can advect a fluid parcel right across the fluid's domain. When the steering level varies strongly with the lateral ordinate, the problem on each horizontal level is more similar to that of a two-dimensional zonal shear flow and Kelvin's cat's eyes will form. For waves whose velocities are of sufficiently large amplitude compared with those due to the lateral shear of the zonal flow these cat's eyes will extend across the whole of the flow and the flow patterns will resemble those studied in this paper.

The non-singular nature of the critical level is the second 'non-generic' feature. There is no particular reason why the contours of constant Q_y should coincide precisely with isotachs of the zonal flow. Hence even if there is a contour on which $Q_y = 0$ the steering level will not usually coincide with it precisely. Neutral modes on such flows have singular values of potential vorticity at the steering level (see (1.6)). As noted in §2 the inner equations allow room for such fields of potential vorticity which are at a lower order than those that dominated the solution of the non-singular problem. It hence seems very likely that for very small values of ΔB the evolution in the critical layer will usually be quite different from that studied in this paper.

The analysis was undertaken despite an appreciation of these points for three reasons. First, it seems worth elucidating the simpler problem first, making it clear that the evolution in the critical layer can be important whether the steering level is singular or not. Secondly the calculation of appropriate singular neutral modes about which to pivot the analysis would by itself require a considerable effort. Finally the neglect of diffusion in singular critical layers would be of doubtful validity in many applications (particularly for rotating annulus experiments). Solutions, like Eady's, which deliberately avoid complexities are usually the most illuminating, particularly when their limitations are clearly understood.

4.4 *Stability of solution*

Figures 4 and 6 show that strong horizontal gradients of potential vorticity develop within the critical layer. There are regions where the gradients are approximately perpendicular to the stream-function contours and of opposite sign above and below the critical level. Killworth & McIntyre (1985) and Haynes (1989) have demonstrated that Stewartson's (1978) analytical solution, which develops similar reversals in potential vorticity gradients, is unstable to waves of small wavelength. It seems unlikely, however, that the solution developed in this paper is subject to similar rapid instabilities. In order to see this, note first that any solution of (2.29) excludes such instabilities because the advecting stream function is forced to be of the form (2.26). Linear perturbations to waves (other than the gravest mode) are conservatively advected by (2.29). Instabilities with a wavenumber k in the x-direction which is higher than that of the basic wave require a perturbation stream function $\delta\psi_1'$ of wavenumber k within the critical layer. If $\delta\psi_1'$ has a steady shape outside the steering level and moves with it, it will have hyperbolic dependence on z outside the critical layer:

$$\psi_1' = \begin{cases} a\cosh\{\alpha^{(k,l)}(z-\frac{1}{2})\}\rho^{(k,l)}(y), & z > 0, \\ a\cosh\{\alpha^{(k,l)}(z+\frac{1}{2})\}\rho^{(k,l)}(y), & z < 0. \end{cases} \tag{4.1}$$

By (2.34), $\phi_{2\zeta\zeta}$ would need to be non-zero to match the jump in ψ_{1z}' across the critical layer. As noted after (2.28), this quantity is zero within a non-singular critical layer. In other words the only normal mode with its steering level at mid-level is that of the basic wave. So the first-order stream function in the critical layer is forced to be proportional to that of the neutral normal mode and instabilities involving higher wavenumbers are only possible in higher-order solutions.

4.5. *Neglect of vertical advection*

The restriction of the solutions of §2 to waves of moderate amplitude also emerges from an examination of the conditions under which the solution satisfies the quasi-geostrophic equations. The neglect of the ageostrophic horizontal velocities requires

$Ro \ll \Delta B$. It is plausible that no qualitative errors would arise from their neglect but as we now show the neglect of vertical velocity advection also requires $Ro \ll B\Delta B$. Let

$$w = Lw^*/(U_0 H) \tag{4.2}$$

be the non-dimensional form of the vertical velocity w^*. Then according to quasi-geostrophic theory

$$w \simeq -\frac{Ro}{B}\frac{\mathrm{D}_g \psi_z}{\mathrm{D}t}. \tag{4.3}$$

In the critical layer

$$\mathrm{D}_g \psi_z/\mathrm{D}t \approx \Delta B \phi_{1x} \Phi_{1y\zeta} \tag{4.4}$$

so

$$O\left(\frac{w\partial/\partial z}{u\partial/\partial x}\right) = \frac{Ro}{B^2}\left(\frac{\Delta B}{B}\right)^{-1}. \tag{4.5}$$

Hence the neglect of the vertical advection of potential vorticity in (2.29) (in particular of a term of the form $w\phi_{\zeta\zeta\zeta}/\Delta B$) compared with the horizontal advection requires that $Ro \ll B^2\,(\Delta B/B)$.

Note, however that this condition concerns the validity of the quasi-geostrophic equations. The conservation of potential vorticity in these equations is simply an analogue of the conservation of Ertel potential vorticity following parcels on isentropic surfaces. Hence (4.5) need not be viewed as a necessary condition for evolution in a critical layer to be relevant.

4.6. *Effects of diffusive fluxes*

Diffusive transports have been deliberately neglected (or in the numerical solutions minimized) to this point in the interest of formulating a well-posed problem. A zonal flow which is laterally sheared at the horizontal boundaries will, in a viscous fluid, induce Ekman pumping of axisymmetric vertical motion which will affect the whole of the flow. The stability of such a zonal flow with its meridional circulation is a major problem in its own right.

Diffusion will, of course, play a dominant role in the critical layer (Drazin & Reid 1981, p. 421) when the wave amplitude is small enough. Conditions under which advection dominates diffusion may be found by inserting the scaling used in §2 into the diffusive version of the potential vorticity equation, which in dimensional form is

$$\frac{\mathrm{D}_g^* q^*}{\mathrm{D}t^*} = \left(\nu^* \nabla_h^{*2} + \frac{\kappa^* f^2}{N^2}\frac{\partial^2}{\partial z^{*2}}\right)\nabla_3^{*2}\psi^*. \tag{4.6}$$

At $O(\Delta B^2)$ in the critical layer one obtains

$$\Delta B^2 \frac{\mathrm{D}_g B p_1}{\mathrm{D}t} = \frac{\kappa L^2}{\Delta B H^2}\phi_{3\zeta\zeta\zeta\zeta} + \Delta B\left(\kappa + \frac{\nu B L^2}{H^2}\right)\nabla_h^2 \phi_{3\zeta\zeta} + \Delta B\, \nu B\, \nabla_h^4 \phi_1, \tag{4.7}$$

where

$$\nu = \nu^*/(U_0 L) \quad \text{and} \quad \kappa = \kappa^*/(U_0 L). \tag{4.8}$$

The inviscid critical layer theory requires

$$\frac{\kappa L^2}{H^2 B^3} \ll \left(\frac{\Delta B}{B}\right)^3, \quad \frac{\kappa}{B} + \frac{\nu L^2}{H^2} \ll \left(\frac{\Delta B}{B}\right) \quad \text{and} \quad \nu \ll \Delta B. \tag{4.9}$$

The generation of sharp gradients of Bp_1 within the critical layer makes dissipative processes important even when $\Delta B/B$ is large enough for them to be formally small according to the above scaling arguments. Diffusive transports will control the total enstrophy within the critical layer and dissipate the strongest gradients of Bp_1. Figure 7 shows that even when (4.9) is satisfied by several orders of magnitude, diffusive fluxes limit the gradients of Bp_1 as soon as the wave reaches its first maximum in amplitude.

4.7. *Two-layer fluid experiments*

The order of the transition in two-layer experiments (Hart 1979) is qualitatively different from that found in thermally forced experiments (White 1988). As the inverse Froude number (the analogue of the Burger or thermal Rossby number) is decreased the two-layer system passes from axisymmetric flow to steady waves and then to amplitude-modulated waves. In the thermally forced experiments the transition is usually from axisymmetric flow to amplitude vacillations and then steady waves. Hart (1972) has investigated the lateral structure of the two-layer flows. He argues that each layer's depth-independent axisymmetric zonal flow is arrested by a Stewartson type $E^{\frac{1}{4}}$ layer (E being the Ekman number) whilst the zonal motions of wave perturbations are halted by a viscous Stokes layer. The latter is thinner than the Stewartson layer in most experiments so that much of the axisymmetric flow's lateral shear in its side boundary layer should probably be viewed as being within the inviscid domain of the perturbation field. For a wave with a phase velocity intermediate between those of the two layers, the arguments of §1 imply that the wave amplitude will be governed by Landau's equation which supports steady waves but not amplitude vacillations. Strongly nonlinear evolution in one of the layers will only occur if the layer's zonal velocity happens to coincide with the wave's phase speed. Whilst there are particular cases in which this occurs (Pedlosky 1982*b*; Warn & Gauthier 1989) along most of the axisymmetric transition it does not.

5. Applicability to rotating annulus experiments

Laboratory experiments with rotating annuli are well known and have been reviewed by several authors (e.g. Read 1988). In brief, they concern a fluid contained within a concentric cylindrical annulus whose inner and outer sidewalls are conductors and whose base and lid are insulators. All the walls of the container are rotated together at a uniform rate Ω and a constant temperature difference ΔT is imposed between the outer and inner walls. For a given apparatus the post-transient flows which can be obtained depend chiefly on the thermal Rossby number Θ and the Taylor number Ta:

$$\Theta = g\alpha\Delta TH/(\Omega^2 L^2); \quad Ta = 4\Omega^2 L^5/(\nu^{*2} H). \tag{5.1}$$

For values of $\Theta > 2$ the flow evolves to an axisymmetric state on which only 'weak' waves are found. Providing $Ta > 10^6$, on slowly decreasing Θ a sharp transition, called the upper axisymmetric transition (UAT), to large-amplitude azimuthally varying waves is found. These waves draw their energy from the available potential energy of the stably stratified baroclinic thermal field (Hide & Mason 1975).

Figures 8 and 9 display horizontal cross-sections of (q–g evaluations of) the p.v. field from the numerical simulation of an amplitude-vacillating flow close to the UAT reported in §6(*c*) of Hignett *et al.* (1985). Figure 8 presents the p.v. on the model level

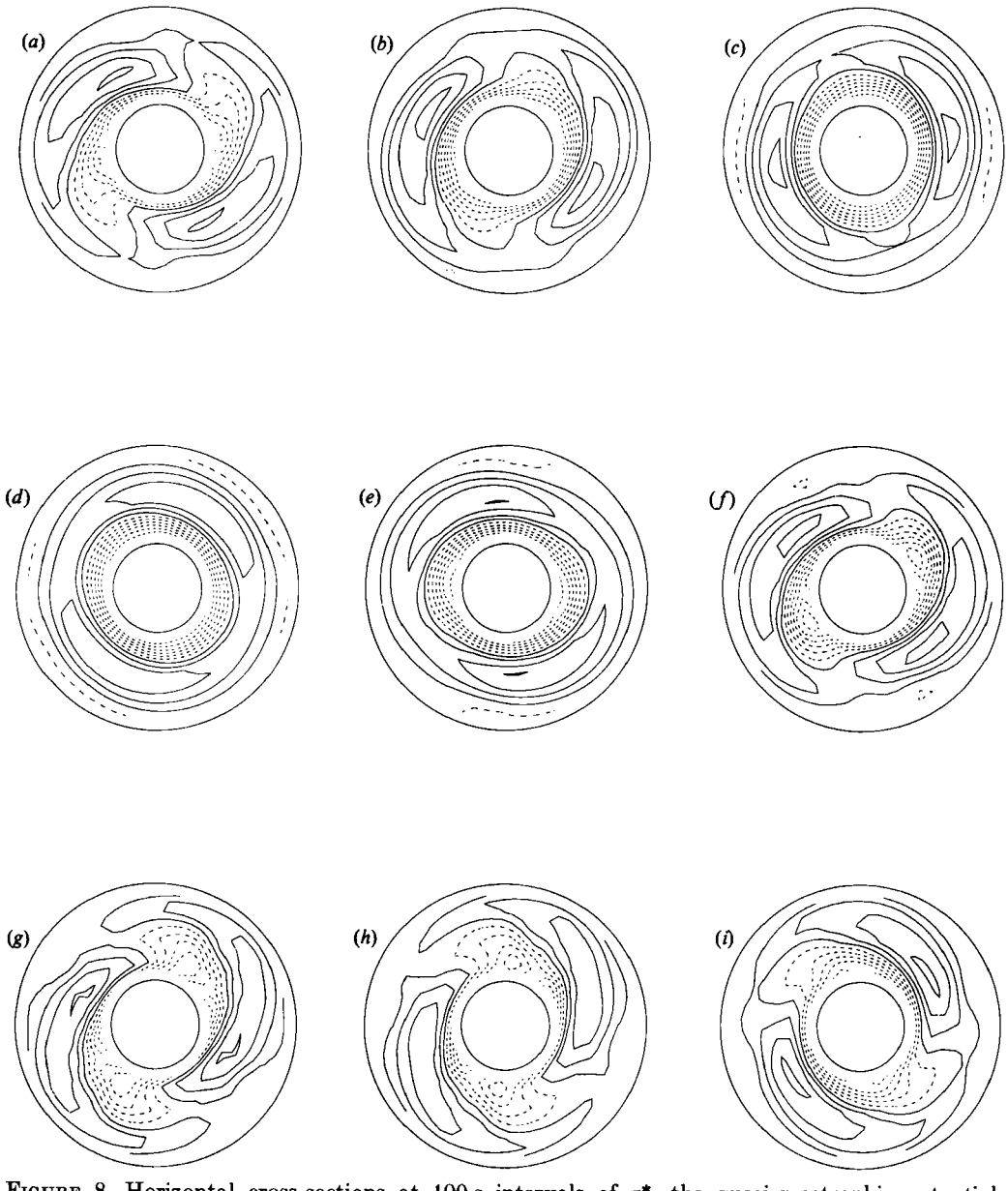

FIGURE 8. Horizontal cross-sections at 100 s intervals of q^*, the quasi-geostrophic potential vorticity field, from a numerical simulation of an amplitude-vacillating flow using the Navier–Stokes model described by Hignett *et al.* (1985). The inner and outer radii and depth of the annulus are 2.5, 8.0 and 14.0 cm respectively and the model has 64 (azimuthal) × 16 (radial) × 16 (vertical) points. The sections are taken on model level 8 which is 5.77 cm above the base, the contour interval is 0.1 s^{-1} and negative contours are dashed.

nearest the steering level at 100 s intervals (the vacillation period is about 600 s). Nonlinear advection of the potential vorticity field is clearly apparent in the asymmetrical and curled contours. Figure 9, which presents the p.v. and stream-function fields on the same level and the p.v. field near the base of the annulus over a period containing the maximum amplitude of the wave, shows that the p.v. field

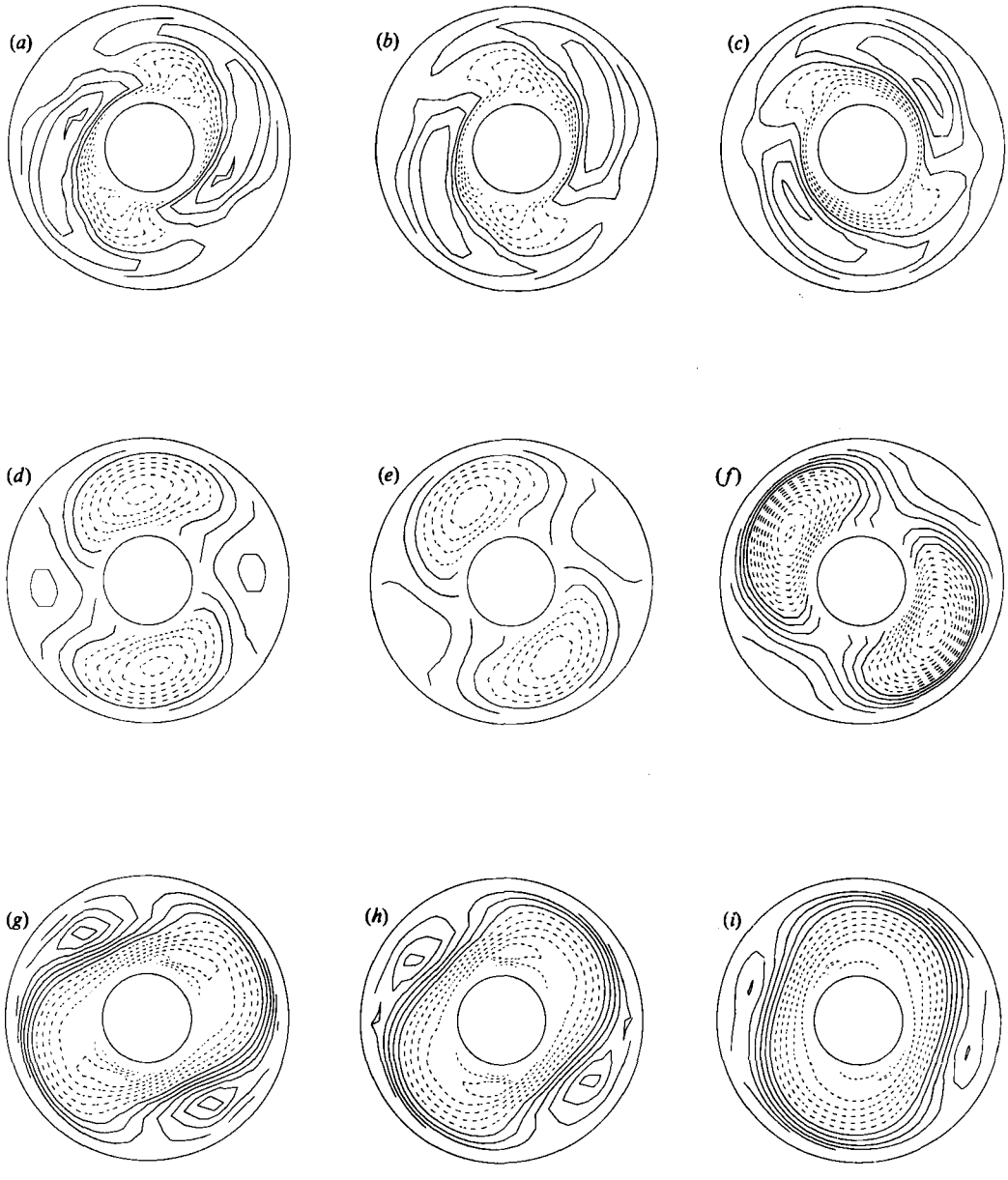

FIGURE 9. (*a*), (*b*) (*c*) A re-display of q^* at 5.77 cm above the base as presented in figure 8 (*g*), (*h*) and (*i*) respectively. (*d*), (*e*) and (*f*) The pressure at the same level and (*g*), (*h*) and (*i*) q^* at 2.00 cm above the base (model level 6) for the corresponding times. The contour interval is 5×10^{-3} N m^{-2} in (*d*), 2×10^{-3} N m^{-2} in (*e*) and (*f*) and 0.2 s^{-1} in (*g*)–(*i*). Negative contours are again dashed.

away from the steering level and the stream function have a much less rich harmonic structure.

Although figures 8 and 9 suggest that nonlinear advection of p.v. is confined to a narrow layer of the flow, it is not clear that the work of §§2 and 3 provides the most appropriate description of waves near the UAT. The main problems in applying the theory concern the form of the axisymmetric flow, the parametric location of the

UAT and the role of diffusive fluxes in the critical layer. These are now discussed in turn.

The form of the velocity profile (2.5) was motivated by cross-sections of the thermal and zonal velocity fields obtained in numerical simulations of the axisymmetric flow near the UAT (see Bell & White 1988, figure 1, for examples of the U, T and 'Q_y' cross-sections). Unfortunately, non-generic aspects of (2.5) (see §4), which simplified the analysis, raise doubts about its applicability. The surface on which $U = c_r$ is fairly flat, but the analogue of the $Q_y = 0$ surface (see Bell & White 1988, figure 1*c*) follows the slope of the isotherms and intersects the isotach $U = c_r$ of the zonal flow quite steeply. Thus the analysis in terms of non-singular critical layers may not be appropriate.

The transitional value of the Burger number according to (2.5) with $a_s = 0.5$, is about 1.5, corresponding to a value for $\Theta = 6$. This value is well into the weak wave regime at the Taylor numbers which can be explored with greatest control in the laboratory. For the Eady profile, inclusion of Ekman pumping brings the Burger number and wavenumber at the transition to unstable normal modes into good agreement with experimental results for the UAT and it is probable that similar improvements in agreement could be made for the laterally shcared flow. Evaluation of this point is complicated, however, by the axisymmetric vertical velocity induced by Ekman pumping in the presence of a laterally sheared flow.

Conditions for the diffusive fluxes within the critical layer to be formally small are provided by (4.9). Using values appropriate for the simulation depicted in figures 8 and 9 ($L = 5$ cm, $H = 15$ cm, $\nu^* = 1.6 \times 10^{-2}$, $\kappa^* = 1.3 \times 10^{-3}$, $U_0 \approx 0.5$ cm s^{-1}, $B \approx 0.5$) and (4.8)

$$\nu/B \approx 10^{-2}, \quad \kappa L^2/(H^2 B^3) \approx 5 \times 10^{-4}. \tag{5.2a, b}$$

$\Delta B/B$ and $(\Delta B/B)^3$ can be estimated as follows. Judging from figure 11 (*c*) of Hignett *et al.* (1985) the time, τ_d, required for their two-lobe wave to double in amplitude is about 100 s. The corresponding initial growth rate $k\, c_i$ of the wave studied in §2 is

$$kc_i = nr\pi c_i \approx \tfrac{1}{2} nr\pi\, \Delta B/B_0, \tag{5.3}$$

where n is the number of wave lobes and the estimate of $c_i = \Delta B\, c_1$ follows from (B 7) and the remark following it. τ_d (which is dimensional) is thus related to $\Delta B/B$ by

$$\tau_d = \frac{\ln 2}{kc_i}\frac{L}{U_0} \approx \frac{\ln 2}{n}\frac{2}{r\pi}\frac{L}{U_0}\frac{1}{\Delta B/B_0}. \tag{5.4}$$

For the amplitude vacillation simulation $r \approx 1/\pi$ and $n = 2$; thus

$$\Delta B/B \approx 7 \times 10^{-2}, \quad (\Delta B/B)^3 \approx 3 \times 10^{-4}. \tag{5.5a, b}$$

Comparison of (5.2) and (5.5) with (4.9) shows that the first of conditions (4.9) is not properly satisfied. Thus it may be more appropriate to compare a diffusive critical layer than an advective one with the annulus flow. Vertical thermal diffusion is likely to be of even greater importance in flows with singular critical levels (i.e. $Q_y \neq 0$ where $U = c_r$).

Comparison of (3.1) and (4.9) suggests that the most appropriate expression for ν_d to use for comparison with laboratory experiments is

$$\nu_d = (\kappa/B + \nu L^2/H^2)\,(B/\Delta B). \tag{5.6}$$

Using the same values as in obtaining (5.2) gives $\nu_d = 3 \times 10^{-2}$. The simulation with ν_d as small as 2×10^{-4} had a marked effect on the evolution of Bp_1, limiting the

tightening of contours, so we conclude that diffusive influences severely limit the evolution within the critical layer in the annulus experiments. An inviscid description might suit part of an amplitude-vacillation cycle but is not able to describe the maintenance of vacillation cycles.

Increasing the Prandtl number of the fluid and/or the aspect ratio will tend to reduce the influence of diffusion in the critical layer, increasing the range of values of $\Delta B/B$ over which (4.9) holds and reducing the effective value of ν_d. Jonas (1981) reports that the fraction of the (Θ, Ta)-regime diagram occupied by amplitude-vacillating flows increases with the Prandtl number, and D. W. Johnson (private communication) has found amplitude vacillation to become more widespread as the aspect ratio (H/L) is increased. These results are consistent with those of Pfeffer, Buzyna & Kung (1980) for fluids with Prandtl numbers of 21 and 73.

In closing we note that improved numerical simulations and further diagnostics of the annulus experiments are desirable. Only 16 vertical levels were used in the above numerical experiment. Since the vertical grid of the model is deliberately stretched to resolve the horizontal and side boundary layers the vertical resolution near mid-level is poor. Even at moderate supercriticalities it would be desirable to use 32 or 64 points in the vertical to obtain a good resolution in the neighbourhood of the steering level.

6. Concluding remarks

The growth of weakly unstable inviscid waves on laterally sheared baroclinic zonal flows has been argued (in §1) to be arrested by the self-advection of their p.v. fields within 'critical' layers centred on the waves' steering levels. Waves growing on flows with uniform p.v. gradients and inviscid waves on laterally uniform flows are arrested by other, weaker, nonlinear interactions. Most 'naturally' occurring baroclinic zonal flows will have substantial lateral shears. We contend that wave disturbances to them will be mainly controlled by the self-advection within their critical layers.

A comparatively simple and special case in which the critical layer is non-singular has been studied in some detail (§§2 and 3). The self-advection severely distorts the original p.v. structure within the critical layer generating some large p.v. gradients. These gradients make local diffusive fluxes much stronger than standard scale analysis would suggest. Detailed studies of less special critical layers on baroclinic flows could be very valuable.

P.v. diagnostics from a numerical simulation of an amplitude-vacillating flow in a rotating annulus (figures 8 and 9) show that as the wave grows its p.v. field is significantly distorted near mid-level. We suggest that the growth phase may be characterized by almost inviscid nonlinear advection of p.v. within the wave's critical layer. During the wave's decay phase diffusive fluxes are probably important in eroding sharp p.v. gradients in the critical layer and re-establishing the axisymmetric flow. Further diagnostics of the roles of advection and dissipation in the critical layer in both laboratory and numerical experiments are needed to establish whether these suggestions are substantially correct.

An early version of this paper formed part of the author's Ph.D. thesis undertaken through the Public Research Institute Scheme at Imperial College, London and the UK Meteorological Office. It is a pleasure to thank R. Hide, P. L. Read and A. A. White for their advice, encouragement and assistance.

Appendix A. Derivation of matching condition (2.19)

This appendix shows that the condition for (2.17)–(2.19) to have solutions may be expressed as (2.20). Equations (2.17)–(2.19) are

$$\left.\begin{aligned} &\mathrm{M}_0\psi_{2x} = -B_0/U\nabla_{\mathrm{h}}^2\psi_{1x} - J(\psi_1, B_0\nabla_{\mathrm{h}}^2\psi_1)/U + U_{zz}\psi_{1x}/(B_0 U), \\ &\psi_{2zx} = 0 \quad \text{on} \quad z = \pm\tfrac{1}{2}, \\ &[\psi_2]_{0^-}^{0^+} = H(x,y); \quad [\psi_{2z}]_{0^-}^{0^+} = I(x,y). \end{aligned}\right\} \tag{A 1}$$

The operator M_0 in the first equation above is defined by (2.15) and may be written as

$$\mathrm{M}_0 = \mathrm{M}_1 + \partial^2/\partial z^2; \quad \mathrm{M}_1 \equiv B_0\nabla_{\mathrm{h}}^2 + (BQ_y/U)_{B=B_0}. \tag{A 2}$$

M_1 includes only horizontal derivatives and for the flow (2.5) is independent of depth (see (2.6)). Solutions of (A 1) can hence be expressed as a summation of the eigenfunctions $\rho^{(k,l)}(y)\exp(\mathrm{i}rk\pi x)$ of M_1:

$$\psi_2 = \sum_{k,l} \psi_2^{(k,l)}(z)\rho^{(k,l)}(y)\exp(\mathrm{i}rk\pi x). \tag{A 3}$$

Projection onto the eigenfunctions of M_1 reduces (A 1) to equations of the form

$$\left.\begin{aligned} &\psi_{2zz}^{(k,l)} + \alpha^{(k,l)}\psi_2^{(k,l)} = f^{(k,l)}(z), \\ &[\psi_2^{(k,l)}]_{0^-}^{0^+} = H^{(k,l)}, \quad [\psi_{2z}^{(k,l)}]_{0^-}^{0^+} = I^{(k,l)}, \\ &\psi_{2z}^{(k,l)} = 0 \quad \text{at} \quad z = \pm\tfrac{1}{2} \end{aligned}\right\} \tag{A 4}$$

in which $\alpha^{(k,l)} > 0$ for all modes other than the neutral mode, ρ_{S}, for which $\alpha^{(k,l)} = 0$.

When $\alpha^{(k,l)} > 0$ the complementary solutions enable solutions to be found for any $f^{(k,l)}(z)$, $H^{(k,l)}$ and $I^{(k,l)}$. So it is adequate to consider only the projection into $\rho_{\mathrm{S}}(y)\exp(\mathrm{i}\pi x)$ to find the condition for (A 1) to have a solution. This projection results in a problem of the form

$$\chi_{zz} = E/\sin\pi z + F; \quad [\chi]_{0^-}^{0^+} = R, \quad [\chi_z]_{0^-}^{0^+} = S; \quad \chi_z = 0 \quad \text{at} \quad z = \pm\tfrac{1}{2}, \tag{A 5}$$

in which, for the flow (2.5), χ and F are given by

$$\chi = \iint \rho_{\mathrm{S}}(y)\exp(\mathrm{i}r\pi x)\psi_{2x}\,\mathrm{d}x\,\mathrm{d}y, \quad F = -\pi^2/B_0 \iint \rho_{\mathrm{S}}(y)\exp(\mathrm{i}r\pi x)\psi_{1x}\,\mathrm{d}x\,\mathrm{d}y. \tag{A 6}$$

(Explicit formulae for E, R and S are not needed below.) Integrating (A 5) once yields

$$\left.\begin{aligned} \chi_z &= E/\pi \ln|\tan\tfrac{1}{2}\pi z| + F(z-\tfrac{1}{2}), \quad z > 0, \\ \chi_z &= E/\pi \ln|\tan\tfrac{1}{2}\pi z| + F(z+\tfrac{1}{2}), \quad z < 0, \end{aligned}\right\} \tag{A 7}$$

and hence

$$[\chi_z]_{-z}^{z} = F(2z-1) \to -F \quad \text{as} \quad z \downarrow 0. \tag{A 8}$$

This condition on the jump in potential temperature across the critical layer provides a relationship between the inner and outer solutions which must be satisfied if the solution sought is to be valid. It is the only consistency condition at this order because the complementary solution $\chi = \text{const.}$ can accommodate any jump R in the stream function. Equation (2.20) is easily obtained by substituting (A 6) into (A 8).

Appendix B. Initial conditions

In this Appendix an expression is found for the linearly unstable normal mode in the critical layer, which serves as the initial condition for the numerical simulations of §3.

We start by linearizing (2.1) about the zonal flow (2.5),

$$q'_t + Uq'_x + Q_y \psi'_x = 0, \tag{B 1}$$

and letting $B = B_0 - \Delta B$ and

$$\psi' = \mathrm{Re}\{\rho(y,z)\exp[\mathrm{i}r\pi(x-ct)]\}. \tag{B 2}$$

Posing an expansion for ρ and c in powers of ΔB:

$$\rho = \Delta B \rho_S(y) + \Delta B^2 \rho_1 + \ldots; \quad c = \Delta B c_1 + \ldots, \tag{B 3}$$

based on the neutral normal mode ρ_S,

$$(\mathrm{d}^2/\mathrm{d}y^2 - r^2\pi^2)\rho_S + (Q_y/U)\rho_S = 0, \quad \rho_S = 0 \quad \text{at} \quad y = 0, 1, \tag{B 4}$$

at $O(\Delta B^2)$ one finds that

$$\left.\begin{aligned} &\left(B_0 \nabla_h^2 + \frac{\partial^2}{\partial z^2} + \frac{B_0 Q_y}{U}\right)\rho_1 = -\frac{\pi^2}{B_0}\rho_S - B_0 c_1 \frac{(Q_y/U)\rho_S}{U-c} \\ &\rho_{1z} = 0 \quad \text{on} \quad z = \pm\tfrac{1}{2}; \quad \rho_1 = 0 \quad \text{on} \quad y = 0, 1. \end{aligned}\right\} \tag{B 5}$$

The Fredholm condition for (B 5) to have a solution is that the free (complementary) solution ρ_S be orthogonal to the forcing of ρ_1. This condition determines the dependence of c_1 on ΔB. Standard manipulations show that c_1 is pure imaginary and that

$$\iint \rho_S^2 \pi^2 / B_0 \,\mathrm{d}y\,\mathrm{d}z = -\iint c_1 \frac{B_0 (Q_y/U)\rho_S^2}{U-c}\,\mathrm{d}y\,\mathrm{d}z = \pi |c_1| \int_y \frac{B_0 (Q_y/U)\rho_S^2}{|U_z|_{z=0}}\,\mathrm{d}y. \tag{B 6}$$

So

$$c_1 = \frac{\mathrm{i}T}{2B_0^2}; \quad T = \frac{\displaystyle\int \pi^2 \rho_S^2 \,\mathrm{d}y}{\displaystyle\int \rho_S^2 (Q_y/U)(1 - a_S + a_S \sin \pi y)^{-1}\,\mathrm{d}y}. \tag{B 7}$$

The ratio $T = B_0$ when $a_S = 0$ and is not far from 1 for a_S near 0.5.

Manipulation of (2.29) using (2.30), (2.26), (2.6) and (2.8) shows that $\phi'_{3\zeta\zeta}$ for this normal mode satisfies

$$(U-c)\phi_{3\zeta\zeta x} = B_0 (Q_y/U)\phi'_{1r}. \tag{B 8}$$

So the normal mode with an initial outer stream function of small amplitude γ,

$$\phi'_1 = \cos(r\pi x)\rho_S(y), \tag{B 9}$$

has accompanying vertical variation

$$\phi'_{3\zeta\zeta} = \frac{B_0 (Q_y/U)\rho_S}{|\tilde{U}-c|^2}\{|c|^2 \cos(r\pi x) + \tilde{U}|c| \sin(r\pi x)\}, \tag{B 10}$$

in which

$$c = \Delta B c_1; \quad \tilde{U} = \tfrac{1}{2}\Delta B \pi \zeta (1 - a_S + a_S \sin \pi y). \tag{B 11}$$

Equations (2.37)–(2.40) are simply re-statements of (B 7) and (B 9)–(B 11).

REFERENCES

BELL, M. J. 1989 Theoretical investigations prompted by experiments with baroclinic fluids. Ph.D. thesis, University of London, 215 pp.

BELL, M. J. & WHITE, A. A. 1988 The stability of internal baroclinic jets: some analytical results. *J. Atmos. Sci.* **45**, 2571–2590.

CHARNEY, J. G. 1947 The dynamics of long waves in a baroclinic westerly current. *J. Met.* **4**, 135–162.

CHARNEY, J. G. & STERN, M. E. 1962 On the stability of internal baroclinic jets in a rotating atmosphere. *J. Atmos. Sci.* **19**, 159–172.

CHURILOV, S. M. & SHUKHMAN, I. G. 1987 The nonlinear development of disturbances in a zonal shear flow. *Geophys. Astrophys. Fluid Dyn.* **38**, 145–175.

DRAZIN, P. G. 1970 Non-linear baroclinic instability of a continuous zonal flow. *Q. J. R. Met. Soc.* **96**, 667–676.

DRAZIN, P. G. 1972 Nonlinear baroclinic instability of a continuous zonal flow of viscous fluid. *J. Fluid Mech.* **55**, 577–587.

DRAZIN, P. G. & REID, W. H. 1981 *Hydrodynamic Stability.* Cambridge University Press, 525 pp.

EADY, E. T. 1949 Long waves and cyclone waves. *Tellus* **1**, 33–52.

FELDSTEIN, S. B. & HELD, I. M. 1989 Barotropic decay of baroclinic waves in a two-layer beta-plane model. *J. Atmos. Sci.* **46**, 3416–3430.

HALTINER, G. J. & WILLIAMS, R. T. 1980 *Numerical Prediction and Dynamic Meteorology.* Wiley, 477 pp.

HART, J. E. 1972 A laboratory study of baroclinic instability. *Geophys. Fluid Dyn.* **3**, 181–209.

HART, J. E. 1979 Finite amplitude baroclinic instability. *Ann. Rev. Fluid Mech.* **11**, 147–172.

HAYNES, P. H. 1989 The effect of barotropic instability on the nonlinear evolution of a Rossby wave critical layer. *J. Fluid Mech.* **207**, 231–266.

HIDE, R. & MASON, P. J. 1975 Sloping convection in a rotating fluid: a review. *Adv. Phys.* **24**, 47–100.

HIGNETT, P. 1985 Characteristics of amplitude vacillation in a differentially heated rotating annulus. *Geophys. Astrophys. Fluid Dyn.* **31**, 247–281.

HIGNETT, P., WHITE, A. A., CARTER, R. D., JACKSON, W. D. N. & SMALL, R. M. 1985 A comparison of laboratory measurements and numerical simulations of baroclinic wave flows in a rotating cylindrical annulus. *Q. J. R. Met. Soc.* **111**, 131–154.

HOSKINS, B. J. & SIMMONS, A. J. 1975 A multi-layer spectral model and the semi-implicit method. *Q. J. R. Met. Soc.* **101**, 637–655.

JAMES, I. N. 1987 Suppression of baroclinic instability in horizontally sheared flows. *J. Atmos. Sci.* **44**, 3710–3720.

JONAS, P. R. 1981 Some effects of boundary conditions and fluid properties on vacillation in thermally driven rotating flow in an annulus. *Geophys. Astrophys. Fluid Dyn.* **18**, 1–23.

KILLWORTH, P. D. & MCINTYRE, M. E. 1985 Do Rossby-wave critical layers absorb, reflect, or over-reflect? *J. Fluid Mech.* **161**, 449–492.

KREYSZIG, E. 1982 *Advanced Engineering Mathematics.* Wiley, 939 pp.

MASLOWE, S. A. 1986 Critical layers in shear flows. *Ann. Rev. Fluid Mech.* **18**, 405–432.

MCINTYRE, M. E. & PALMER, T. N. 1985 A note on the general concept of wave breaking for Rossby and gravity waves. *Pure Appl. Geophys.* **123**, 964–975.

PEDLOSKY, J. 1964 The stability of currents in the atmosphere and the oceans. Part I *J. Atmos. Sci.* **27**, 201–219.

PEDLOSKY, J. 1970 Finite amplitude baroclinic waves. *J. Atmos. Sci.* **27**, 178–200.

PEDLOSKY, J. 1982*a* *Geophysical Fluid Dynamics.* Springer, 624 pp.

PEDLOSKY, J. 1982*b* A simple model for nonlinear critical layers in an unstable baroclinic wave. *J. Atmos. Sci.* **39**, 2119–2127.

PFEFFER, R. L., BUZYNA, G. & KUNG, R. 1980 Relationships among eddy fluxes of heat, eddy temperature variances and basic state temperature parameters in thermally driven rotating fluids. *J. Atmos. Sci.* **37**, 2577–2599.

READ, P. L. 1988 The dynamics of rotating fluids: the 'philosophy' of laboratory experiments and studies of the atmospheric general circulation. *Met. Mag.* **117**, 35–45.

RHINES, P. B. & HOLLAND, W. R. 1979 A theoretical discussion of eddy-driven mean flow. *Dyn. Atmos. Oceans* **3**, 289–325.

RHINES, P. B. & YOUNG, W. R. 1983 How rapidly is a passive scalar homogenized within closed streamlines? *J. Fluid Mech.* **133**, 135–148.

STEWARTSON, K. 1978 The evolution of the critical layer of a Rossby wave. *Geophys. Astrophys. Fluid Dyn.* **9**, 185–200.

WARN, T. & GAUTHIER, P. 1989 Potential vorticity mixing by marginally unstable baroclinic disturbances. *Tellus* **41A**, 115–131.

WARN, T. & WARN, H. 1978 The evolution of a nonlinear critical layer. *Stud. Appl. Maths.* **59**, 37–71.

WHITE, A. A. 1988 The dynamics of rotating fluids: numerical modelling of annulus flows. *Met. Mag.* **117**, 54–63.